Charge density wave like behavior with magnetic ordering in orthorhombic $Sm_2Ru_3Ge_5$

C. N. Kuo,[1] C. J. Hsu,[1] C. W. Tseng,[1] W. T. Chen,[2] S. Y. Lin,[3] W. Z. Liu,[4] Y. K. Kuo,[4,*] and C. S. Lue[1,†]

[1]*Department of Physics, National Cheng Kung University, Tainan 70101, Taiwan*
[2]*Center for Condensed Matter Sciences, National Taiwan University, Taipei 10617, Taiwan*
[3]*Department of Physics, National Chung Cheng University, Chiayi 62102, Taiwan*
[4]*Department of Physics, National Dong Hwa University, Hualien 97401, Taiwan*

(Received 5 November 2019; revised manuscript received 13 February 2020; accepted 13 April 2020; published 28 April 2020)

In order to explore the physical properties of orthorhombic $U_2Co_3Si_5$-type $Sm_2Ru_3Ge_5$, we have carried out a combined study by means of the measurements of the magnetic susceptibility χ, electrical resistivity ρ, Seebeck coefficient S, and specific heat C_p. An antiferromagnetic phase transition at the Néel temperature $T_N \simeq 7$ K has been identified by all measured physical quantities. Remarkably, another intrinsic phase transition characterized by marked features has been discerned at $T^* \simeq 240$ K. The distinct peak in C_p at T^* with the lack of thermal hysteresis behavior provides strong evidence for the second-order phase transition in nature. It is noticed that the observations near T^* are reminiscent of a typical charge density wave (CDW) ordering. We compared the experimental results with those observed in a polymorph of $Sm_2Ru_3Ge_5$ with the tetragonal $Sc_2Fe_3Si_5$-type structure which was recently reported to exhibit the coexistence of magnetic and CDW phase transitions. On this basis, the observed features in orthorhombic $Sm_2Ru_3Ge_5$ have been discussed by comparing with the results in tetragonal $Sm_2Ru_3Ge_5$ as well as other CDW systems.

DOI: 10.1103/PhysRevB.101.155140

I. INTRODUCTION

Ternary intermetallic silicides and germanides with chemical formula $R_2T_3X_5$ (R = rare earth elements; T = transition metals; X = Si, Ge, referred to as "235" compounds) continue to attract attention in the field of condensed matter physics due to the existence of rich electronic and magnetic phenomena. Unconventional superconductivity, complex magnetism, and charge density wave (CDW) behavior have been widely reported in this class of materials. The examples include two-gap superconductivity in $Lu_2Fe_3Si_5$ [1,2], superconductivity with antiferromagnetic (AFM) transition in [3], double phase transitions in $Ce_2Ni_3Ge_5$ and $U_2Ir_3Si_5$ [4,5], and multiple CDW behavior in $Lu_2Ir_3Si_5$ [6–9]. For the crystallographic structure of the 235 compounds, the orthorhombic $U_2Co_3Si_5$-type (space group *Ibam*) and the tetragonal $Sc_2Fe_3Si_5$-type (space group *P*4/*mnc*) are two most common structures [10]. Both structures for $R_2T_3X_5$ were depicted in Figs. 1(a) and 1(b), respectively. The orthorhombic and the tetragonal structures are geometrically similar with the difference mainly due to the bonding between the transition metals and the surrounding atoms. For both structural types, there are two nonequivalent crystallographic sites occupied by T atoms (denoted as $T1$ and $T2$) and three by X atoms ($X1$, $X2$, and $X3$). There is only one site resided in by the rare-earth R atoms. The link of the nearest-neighboring R atoms forms a quasi-one-dimensional (1D) zigzag chain along the c axis; these are well separated from the T-X ring.

The titled compound of $Sm_2Ru_3Ge_5$ has been identified to adopt the orthorhombic $U_2Co_3Si_5$-type structure, according to the early x-ray diffraction (XRD) analysis on the polycrystalline specimen [11]. Nevertheless, this material has received very little attention and various measurements utilized for characterizing its fundamental physical properties have remained lacking. Very recently, a new polymorph of $Sm_2Ru_3Ge_5$ with the tetragonal $Sc_2Fe_3Si_5$-type structure was synthesized [12]. Within the tetragonal structure, $Sm_2Ru_3Ge_5$ has been found to exhibit a ferromagnetic (FM) ordering below the transition temperature $T_C \simeq 7$ K accompanied by a CDW phase transition near $T_{CDW} \simeq 175$ K. The observations bear a striking resemblance to another Sm-based analogue of $SmNiC_2$, which undergoes a FM transition at $T_C \simeq 17.5$ K and a CDW transition at $T_{CDW} \simeq 148$ K [13–15]. The coexistence of the CDW with local moment ferromagnetism in $SmNiC_2$ has been widely investigated, especially focusing on the effects from the external magnetic field and pressure and the possibly induced quantum critical phase transition driven by these parameters [16–19]. The realization of the quantum critical phenomenon is one of the major themes in solid-state physics, and continues to stimulate the search for more systems relevant to the related issue. In this respect, the tetragonal $Sm_2Ru_3Ge_5$ compound would be a promising candidate for the study of the competition between CDW and local ferromagnetism.

As motivated, we have focused on orthorhombic $Sm_2Ru_3Ge_5$ to explore its fundamental physical properties and to examine whether this material exhibits concomitant CDW and magnetic phase transitions. In this work, we have presented various physical properties of the orthorhombic $Sm_2Ru_3Ge_5$ compound including magnetization, electrical

*ykkuo@gms.ndhu.edu.tw
†cslue@mail.ncku.edu.tw

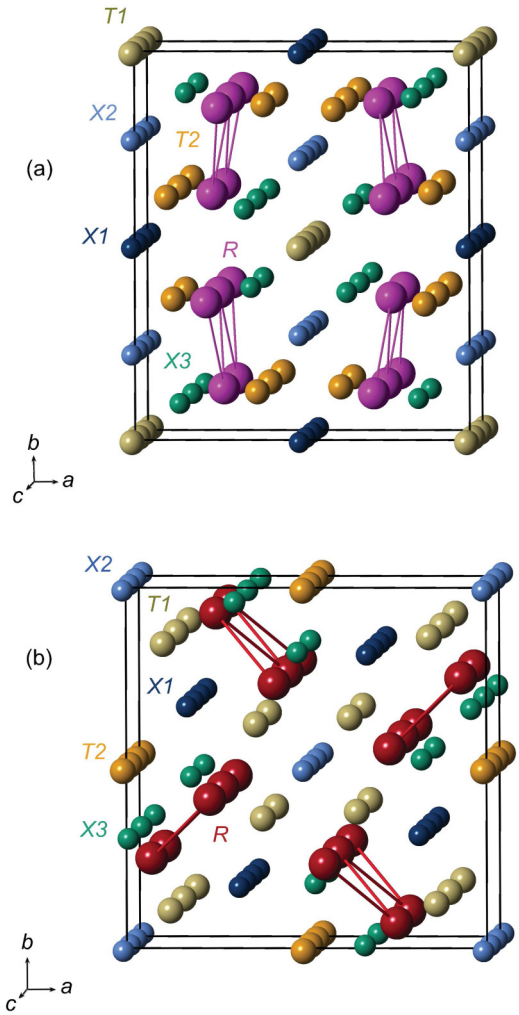

FIG. 1. The orthorhombic $U_2Co_3Si_5$-type (a) and the tetragonal $Sc_2Fe_3Si_5$-type (b) structures of $R_2T_3X_5$ (R = rare earth elements; T = transition metals; X = Si, Ge). The bonds highlight the interaction between the nearest-neighbor R atoms.

resistivity, Seebeck coefficient, and specific heat. An AFM ordering at the Néel temperature $T_N \simeq 7$ K accompanied by a high-temperature phase transition at $T^* \simeq 240$ K has been observed. Since the signatures near T^* are quite similar to those observed in typical CDW materials, the experimental results have been discussed by comparing with the features reported for tetragonal $Sm_2Ru_3Ge_5$ as well as other CDW systems.

II. EXPERIMENT DETAILS

Polycrystalline $Sm_2Ru_3Ge_5$ compound was prepared by arc-melting stoichiometric mixtures of high-purity elements in a Zr-gettered argon atmosphere. Briefly, the mixture of 99.9% Sm, 99.95% Ru, and 99.99% Ge elemental pieces with the stoichiometric ratio was placed in a water-cooled copper hearth. The resulting ingot was turned and remelted at least three times to promote homogeneity. The weight loss during melting is less than 0.5%. The obtained ingot was wrapped in a tantalum foil and annealed in a vacuum-sealed quartz tube at 1100 K for 5 days, followed by furnace cooling. Attempts to obtain the tetragonal phase of $Sm_2Ru_3Ge_5$ by arc-melting with different postannealing treatments failed. According to the phase diagram of Sm-Ru-Ge intermetallics [20], only the orthorhombic phase of $Sm_2Ru_3Ge_5$ has been reported among nine ternary compounds. It thus indicates that $Sm_2Ru_3Ge_5$ with the orthorhombic phase is thermodynamically more stable than with the tetragonal one which should be grown by means of the flux method [12].

The powder x-ray diffraction patterns were collected at Taiwan Photon Source (TPS), National Synchrotron Radiation Research Center (NSRRC), Taiwan. The specimen was pulverized and packed in a 0.1-mm borosilicate capillary to minimize the absorption effect. The capillary was kept spinning during data collection for powder averaging. The patterns were collected with beam energy 15 keV (wavelength $\lambda = 0.826\,56$ Å), where the main diffraction peaks were shown in the presented two theta angle region.

The temperature-dependent magnetic susceptibility and isothermal magnetization between −70 and 70 kOe were measured using a commercial (Quantum Design) superconducting quantum interference device (SQUID). The electrical resistivity ρ was measured using a standard four-probe method. The Seebeck coefficient S measurement was performed in a closed-cycle refrigerator, using a direct heat-pulse technique. The temperature difference was detected by an E-type differential thermocouple with junctions thermally attached to two well-separated positions along the longest direction of the specimen, which was cut into a rectangular parallelepiped shape with dimensions of about $8 \times 3 \times 3\,\text{mm}^3$. The low-temperature specific heat C_p measurement was carried out in a Physical Property Measurement System (PPMS) with a heat-pulsed thermal relaxation calorimeter in the temperature range from 1.8 to 20 K. The high-temperature C_p data between 100 and 300 K were obtained from a home-built ac calorimeter, using chopped light as a heat source.

The first-principles calculations for orthorhombic $Sm_2Ru_3Ge_5$ were performed based on the density functional theory (DFT) using the Vienna *Ab Initio* Simulation Package (VASP) [21,22]. The electron-ion interactions were evaluated by the projector augmented wave (PAW) method [23], in which the electron-electron Coulomb interactions belong to the many-particle exchange and correlation energies under the Perdew-Burke-Ernzerhof (PBE) generalized gradient approximation [24]. Further computational details are presented in the Supplemental Material [25]; also see Refs. [26–29].

III. RESULTS AND DISCUSION

The upper and lower panels of Fig. 2(a) show the results of XRD at room temperature and 100 K, respectively. All diffraction peaks were indexed to the expected *Ibam* phase for orthorhombic $Sm_2Ru_3Ge_5$. As compared with both XRD patterns, we found no structural phase transition between 100 K and room temperature. The Rietveld refinement for the room-temperature XRD patterns is given in Fig. 2(b), yielding the lattice parameters $a = 9.866\,65(4)$, $b = 12.443\,52(5)$, and $c = 5.789\,98(2)$ Å. The obtained values are consistent with those reported in the literature [11]. With the same analysis for the XRD patterns collected at low temperatures,

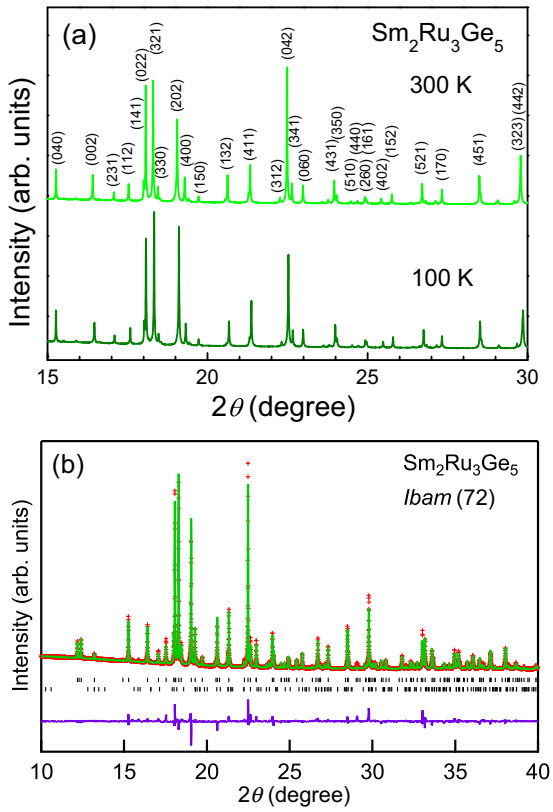

FIG. 2. (a) Synchrotron x-ray diffraction patterns collected at 300 and 100 K for powdered $Sm_2Ru_3Ge_5$. Reflection peaks were indexed with respect to the *Ibam* phase. (b) The Rietveld refinement of $Sm_2Ru_3Ge_5$ XRD patterns collected at 300 K. The red cross and green and purple lines represent the observed pattern, calculated profile, and the difference between the observed and calculated intensities, respectively. The Bragg peaks of $Sm_2Ru_3Ge_5$ and minor Ru_2Ge_3 (of about 4.4 wt%) are shown as black tick marks from top to bottom, respectively.

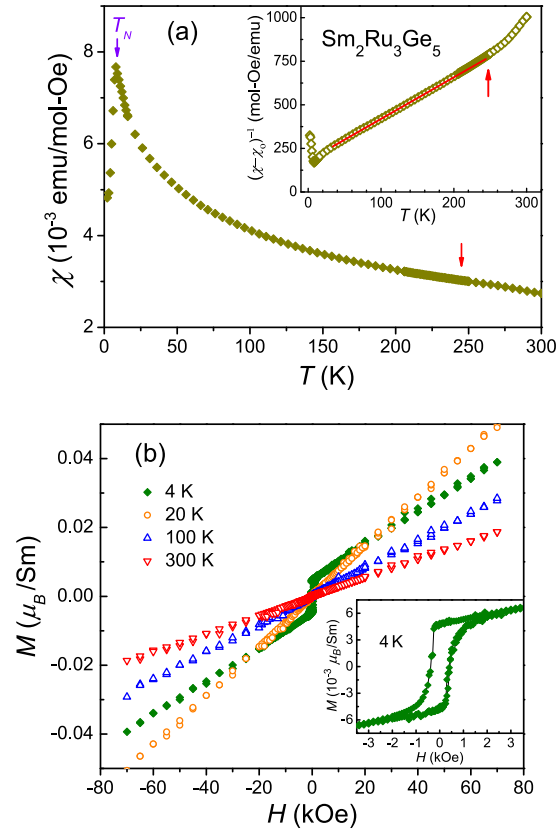

FIG. 3. (a) Temperature dependence of the magnetic susceptibility χ for orthorhombic $Sm_2Ru_3Ge_5$. A cusp at $T_N \simeq 7$ K was marked for the AFM ordering. Inset: A plot of $(\chi - \chi_o)^{-1}$ vs T with a fit to the modified Curie-Weiss expression. The arrow indicates the deviation from the linear behavior. (b) Field-dependent magnetization measured at 4, 20, 100, and 300 K between −70 and 70 kOe. The inset shows an enlarged plot of M vs H obtained at 4 K.

we determined the lattice constants $a = 9.851\,29(4)$, $b = 12.444\,10(4)$, and $c = 5.771\,18(2)$ Å for orthorhombic $Sm_2Ru_3Ge_5$ at 100 K.

The temperature-dependent magnetic susceptibility $\chi(T) = M/H$ of orthorhombic $Sm_2Ru_3Ge_5$ in the range between 2 and 300 K under an external field of 20 kOe is displayed in Fig. 3(a). A sharp cusp at $T_N \simeq 7$ K signifies the occurrence of an AFM ordering. By contrast, the tetragonal $Sm_2Ru_3Ge_5$ compound exhibits a FM phase transition at $T_C \simeq 7$ K [12]. The comparison reveals the essential difference in the spin configuration within the different types of structures for $Sm_2Ru_3Ge_5$. To shed light on the antiferromagnetism of orthorhombic $Sm_2Ru_3Ge_5$, we have performed the calculations with the consideration of the complete pseudopotential with six $4f$ electrons. Accordingly, the AFM ground state is energetically favorable as compared to the FM state. In fact, the orthorhombic $U_2Co_3Si_5$-type structure offers a suitable environment for the AFM state associated with the opposite spin direction of Sm and Ru atoms. On the other hand, the tetragonal $Sc_2Fe_3Si_5$-type structure has a relatively disordered alignment of Sm-Ru bonds. As a consequence, the antiparallel spin configuration does not exist in the tetragonal $Sc_2Fe_3Si_5$-type $Sm_2Ru_3Ge_5$. The computational details are described in the Supplemental Material [25].

We also found that χ obeys a modified Curie-Weiss expression as $\chi = \chi_o + C/(T - \theta_{CW})$ between 25 and 240 K. Here, χ_o is a temperature-independent term, C is the Curie constant, and θ_{CW} is the Curie-Weiss temperature. Based on the linear fit of $(\chi - \chi_o)^{-1}$ to the Curie-Weiss behavior, as demonstrated in the inset of Fig. 3(a), we obtained the parameters of $\chi_o = (1.64 \pm 0.05) \times 10^{-3}$ emu/mol Oe, $C = 0.42 \pm 0.03$ emu K/mol Oe, and $\theta_{CW} = -75 \pm 5$ K. The negative sign of θ_{CW} suggests an effectively AFM coupling between the magnetic moments. From the value of C, we extracted the effective magnetic moment of $1.3 \pm 0.04\,\mu_B$. This is a bit lower than the measured $1.5\,\mu_B$ for the free Sm^{3+} cation. It is apparent that the inverse $\chi - \chi_o$ deviates from the linear behavior as the temperature is higher than 240 K, which was indicated by an arrow in the inset of Fig. 3(a). It is noteworthy that a very recent study of $Er_2Ir_3Si_5$ also revealed a small but distinct change in χ undergoing the CDW transition [30]. Therefore, the present observation is presumably attributed to the CDW formation which would

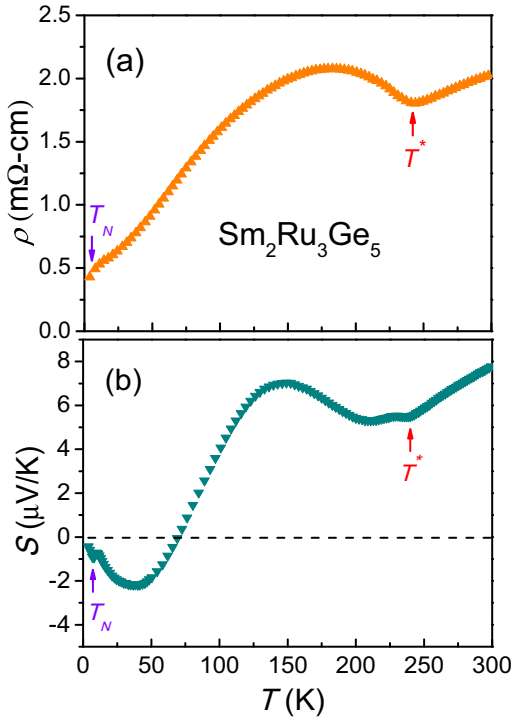

FIG. 4. Temperature variations of the electrical resistivity ρ (a) and Seebeck coefficient S (b) for orthorhombic $Sm_2Ru_3Ge_5$. The arrows indicate the phase transition temperatures of $T_N \simeq 7$ K and $T^* \simeq 240$ K, respectively.

affect the magnitude of the magnetic local moments on Sm^{3+} as observed.

To further identify the AFM ordering at $T_N \simeq 7$ K and examine any magnetic phase transitions at around 240 K, we have carried out the field-dependent magnetization $M(H)$ measured at 4, 20, 100, and 300 K. As demonstrated in Fig. 3(b), M is almost proportional to H and shows no remanent magnetization for the temperature higher than T_N. Such a result confirms the absence of magnetic phase transitions above T_N. On the contrary, the $M(H)$ curve at 4 K exhibits a weak remanent magnetization of $M_r \simeq 0.005\,\mu_B$/Sm. A hysteresis loop with a coercive magnetic field of $H_c \simeq 400$ Oe was clearly seen in the enlarged M vs H plot, as displayed in the inset of Fig. 3(b). For the magnetic field higher than approximately 2 kOe, the $M(H)$ curve becomes linear, commonly observed in the typical AFM systems. It is noted that the magnitude of M_r is much lower than the theoretical saturation magnetization M_s ($\simeq 1\,\mu_B$ in the order of magnitude), suggesting that the observation cannot be attributed to the conventional FM ground state. Instead, the observed FM contribution is very likely due to the existence of a small amount of magnetic impurities in the studied sample.

The temperature variation of electrical resistivity ρ is shown in Fig. 4(a). At low temperatures, a kink feature corresponding to the AFM ordering at $T_N \simeq 7$ K has been discerned. Upon raising the temperature, ρ gradually increases and then exhibits a broad hump near 200 K with an abrupt upturn at $T^* \simeq 240$ K. This is essentially different from the feature in tetragonal $Sm_2Ru_3Ge_5$, which has been ascribed to a conventional semiconductor to a Kondo semiconductor transition across its $T_{CDW} \simeq 175$ K [12]. It is remarkable that the anomalous behavior in the vicinity of T^* resembles a typical CDW phase transition due to the partially gapped Fermi surfaces associated with the CDW formation. Similar electrical resistivity signatures have been reported in various CDW materials such as $Lu_2Ir_3Si_5$, $Lu_5Rh_4Si_{10}$, $RNiC_2$, $LaAuSb_2$, and CuTe [7,31–39].

It is known that the Seebeck coefficient is a sensitive probe for the phenomenon associated with changes in the Fermi surfaces, such as CDW ordering and crystallographic distortion [15,40–47]. The temperature dependence of the measured S for orthorhombic $Sm_2Ru_3Ge_5$ is illustrated in Fig. 4(b). At low temperatures, the sign of S is negative, suggesting that the n-type carriers dominate the thermoelectric transport in orthorhombic $Sm_2Ru_3Ge_5$. A dip feature associated with the AFM ordering was also seen at $T_N \simeq 7$ K. Upon heating, S exhibits a drastic temperature dependence accompanied by a sign reversal above 70 K. The strong temperature variation of S gives evidence for the presence of a multiband effect, which would be responsible for the observations of a broad hump near 140 K and a weak feature at around 220 K. Therefore, the measured Seebeck coefficient can be described as $S = (\sigma_n S_n + \sigma_p S_p)/(\sigma_n + \sigma_p)$, where $S_{n,p}$ and $\sigma_{n,p}$ represent the Seebeck coefficients and electrical conductivities for the n- and p-type carriers from electronic and hole bands, respectively. In principle, each parameter is governed by the scattering relaxation time, which varies differently with temperature. As a result, the positive S at high temperatures can be understood by an increase of the p-type carriers with temperature. In tetragonal $Sm_2Ru_3Ge_5$, the carriers responsible for the transport are dominated by electrons, as suggested by the negative Hall coefficient in the temperature range of 2–300 K [12].

Similar to the observation in ρ, a distinctive feature in S has been noticed in the vicinity of $T^* \simeq 240$ K. This phenomenon can be realized as an increasing contribution from the opposite type of the carriers, presumably arising from a modification in the Fermi surfaces across the phase transition. It is worthwhile mentioning that the anomalous behavior in S resembles those of $RNiC_2$ and $R_5Ir_4Si_{10}$, which have been identified as three-dimensional (3D) CDW compounds [15,48,49]. With this comparison, we pointed out the possible CDW ordering associated with the peculiar phase transition at T^* in the present case of orthorhombic $Sm_2Ru_3Ge_5$.

The low-temperature specific heat C_p exhibits a spiky cusp at around 7 K corresponding to the AFM ordering, as shown in Fig. 5. The analysis of C_p can be used to determine the Sommerfeld coefficient γ and the Debye constant β by means of $C_p(T) = \gamma T + \beta T^3 + \delta T^5$. The first term is the electronic specific heat while the remaining two terms are the phonon contributions. The last one is due to anharmonic effects. We thus plotted C_p/T vs T^2 in the inset of Fig. 5, with a solid curve representing the fitting function. Such a fit yields the values of $\gamma = 3 \pm 1$ mJ/mol K^2, $\beta = 0.90 \pm 0.05$ mJ/mol K^4, and $\delta = (2.7 \pm 0.5) \times 10^{-4}$ mJ/mol K^6. The Debye temperature Θ_D can be derived from β using $\Theta_D = (12\pi^4 ZR/5\beta)^{1/3}$, where $Z = 10$ is the number of atoms per formula unit and $R = 8.314$ J/mol K is the gas constant. The determined $\Theta_D = 278 \pm 5$ K is lower than 337 K reported in tetragonal

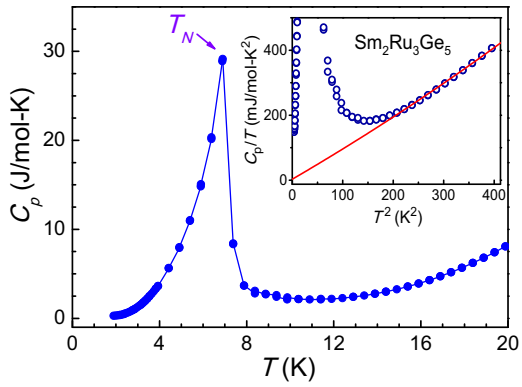

FIG. 5. Temperature dependence of the specific heat C_p for orthorhombic $Sm_2Ru_3Ge_5$. The inset shows a plot of C_p/T vs T^2 with a solid curve which is the fitted function described in the text.

$Sm_2Ru_3Ge_5$ [12]. It is worthwhile mentioning that the obtained γ has a large uncertainty since the huge magnitude of C_p/T in the vicinity of the AFM transition would significantly affect the estimated value. According to the Sommerfeld theory of conduction in metals, the measured γ can be used to estimate the Fermi-level density of states (DOS) $D(\varepsilon_F)$ via $\gamma = \pi^2 k_B{}^2 D(\varepsilon_F)/3$, where k_B is the Boltzmann constant and ε_F is the Fermi energy. Therefore, a small value of $D(\varepsilon_F) = 1.26 \pm 0.42$ states/eV for orthorhombic $Sm_2Ru_3Ge_5$ was deduced. This is in agreement with the calculated result, indicating a deep valley in the DOS near ε_F, as illustrated in Fig. 1S(b) of the Supplemental Material [25].

The temperature dependence of C_p between 100 and 300 K for orthorhombic $Sm_2Ru_3Ge_5$ is given in Fig. 6. The presence of an evident peak in C_p demonstrates the appearance of an intrinsic phase transition at $T^* \simeq 240$ K. The absence of thermal hysteresis indicates that this phase transition is second order in nature. The peak feature is less pronounced as compared to that in tetragonal $Sm_2Ru_3Ge_5$, which has been ascribed by the CDW formation [12]. To evaluate the change of the entropy ΔS associated with the phase transition, we first determined

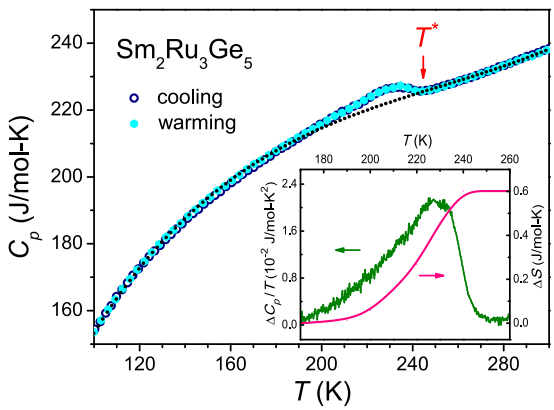

FIG. 6. Temperature-dependent C_p for orthorhombic $Sm_2Ru_3Ge_5$ measured during cooling and warming processes in a high-temperature region. Inset: A plot of $\Delta C_p/T$ vs T and the corresponding entropy change ΔS associated with the phase transition around T^*.

the excess specific heat ΔC_p by subtracting a smooth background, estimated by fitting the lattice specific heat through the experimental data far from the transition region. The temperature dependence of $\Delta C_p/T$ around the phase transition is shown in the inset of Fig. 6. The corresponding $\Delta S \simeq 0.6$ J/mol K was obtained by integrating $\Delta C_p/T$ through the entire phase transition region. In tetragonal $Sm_2Ru_3Ge_5$, the spiky jump in C_p at $T_{CDW} \simeq 175$ K yields a larger entropy change of the CDW, $\Delta S_{CDW} \simeq 1.3$ J/mol K [12]. As a matter of fact, weak features in ΔC_p leading to smaller entropy changes have been reported in various CDW systems such as $LaAgSb_2$, $La_{0.6}Ce_{0.4}Sb_2$, and $TbGe_{2.85}$ [40,50,51].

The present investigation provides strong evidence for an intrinsic phase transition at $T^* \simeq 240$ K in the orthorhombic $U_2Co_3Si_5$-type $Sm_2Ru_3Ge_5$ compound in addition to an AFM phase transition at $T_N \simeq 7$ K. Since the XRD measurements below and above 240 K revealed the absence of a structural transformation in this material, the speculated structural phase transition associated with the peculiar behavior has been ruled out. Also, the phase transition is not likely driven by magnetic ordering because the magnetic susceptibility exhibits no appreciable anomaly around the transition region. The observation could be explained by the fact that the large local moment contribution from Sm^{3+} ions overwhelms any changes in the Pauli paramagnetism. Similar interpretations have been employed in the CDW systems with magnetic ordering such as $SmNiC_2$ and $Er_5Ir_4Si_{10}$ [15,52,53]. Therefore, the mechanism for the observed phase transition is presumably attributed to the electronic origin and/or electron-lattice coupling such as the scenario for the formation of a CDW state driven by Fermi surface nesting. While the signatures near T^* resemble the CDW ordering in many aspects, the unambiguous CDW state in orthorhombic $Sm_2Ru_3Ge_5$ will have to wait until the identification of charge modulation along a specific wave vector direction by means of high-resolution transmission electron microscopy (HRTEM) [8,54].

IV. CONCLUSIONS

In summary, orthorhombic $Sm_2Ru_3Ge_5$ undergoing an AFM transition at $T_N \simeq 7$ K and a second-order phase transition at $T^* \simeq 240$ K has been established by various bulk property measurements. We obtained evidence that the characteristics of the phase transition near T^* are essentially associated with the electronic origin, reminiscent of the scenario for the CDW formation. The comparison of the observed features with those in tetragonal $Sm_2Ru_3Ge_5$ has provided more insights into the intriguing phase transition for both materials. Hence, the orthorhombic $Sm_2Ru_3Ge_5$ compound named in the title appears to be a promising system for the further investigation of the mechanism behind the speculated CDW phase and the interplay between the possible CDW and magnetic ground states.

ACKNOWEDGMENT

This work was supported by the Ministry of Science and Technology of Taiwan under Grants No. MOST-106-2112-M-006-013-MY3 (CSL) and No. MOST-106-2112-M-259-002-MY3 (YKK).

[1] Y. Nakajima, T. Nakagawa, T. Tamegai, and H. Harima, Phys. Rev. Lett. **100**, 157001 (2008).

[2] P. K. Biswas, G. Balakrishnan, D. McK. Paul, M. R. Lees, and A. D. Hillier, Phys. Rev. B **83**, 054517 (2011).

[3] N. H. Sung, C. J. Roh, K. S. Kim, and B. K. Cho, Phys. Rev. B **86**, 224507 (2012).

[4] Z. Hossain, S. Hamashima, K. Umeo, T. Takabatake, C. Geibel, and F. Steglich, Phys. Rev. B **62**, 8950 (2000).

[5] D. X. Li, F. Honda, A. Miyake, Y. Homma, Y. Haga, A. Nakamura, Y. Shimizu, A. Maurya, Y. J. Sato, M. Tokunaga, and D. Aoki, Phys. Rev. B **99**, 054408 (2019).

[6] Y. Singh, D. Pal, S. Ramakrishnan, A. M. Awasthi, and S. K. Malik, Phys. Rev. B **71**, 045109 (2005).

[7] Y. K. Kuo, K. M. Sivakumar, T. H. Su, and C. S. Lue, Phys. Rev. B **74**, 045115 (2006).

[8] M. H. Lee, C. H. Chen, M.-W. Chu, C. S. Lue, and Y. K. Kuo, Phys. Rev. B **83**, 155121 (2011).

[9] N. S. Sangeetha, A. Thamizhavel, C. V. Tomy, S. Basu, A. M. Awasthi, P. Rajak, S. Bhattacharyya, S. Ramakrishnan, and D. Pal, Phys. Rev. B **91**, 205131 (2015).

[10] D. E. Bugaris, C. D. Malliakas, S. L. Bud'ko, N. P. Calta, D. Y. Chung, and M. G. Kanatzidis, Inorg. Chem. **56**, 14584 (2017), and references therein.

[11] G. Venturini, M. Meot-Meyer, J. F. Mareche, B. Malaman, and B. Roques, Mater. Res. Bull. **21**, 33 (1986).

[12] D. E. Bugaris, C. D. Malliakas, F. Han, N. P. Calta, M. Sturza, M. J. Krogstad, R. Osborn, S. Rosenkranz, J. P. C. Ruff, G. Trimarchi, S. L. Bud'ko, M. Balasubramanian, D. Y. Chung, and M. G. Kanatzidis, J. Am. Chem. Soc. **139**, 4130 (2017).

[13] S. Shimomura, C. Hayashi, G. Asaka, N. Wakabayashi, M. Mizumaki, and H. Onodera, Phys. Rev. Lett. **102**, 076404 (2009).

[14] A. Wolfel, L. Li, S. Shimomura, H. Onodera, and S. van Smaalen, Phys. Rev. B **82**, 054120 (2010).

[15] J. H. Kim, J.-S. Rhyee, and Y. S. Kwon, Phys. Rev. B **86**, 235101 (2012).

[16] N. Hanasaki, Y. Nogami, M. Kakinuma, S. Shimomura, M. Kosaka, and H. Onodera, Phys. Rev. B **85**, 092402 (2012).

[17] B. Woo, S. Seo, E. Park, J. H. Kim, D. Jang, T. Park, H. Lee, F. Ronning, J. D. Thompson, V. A. Sidorov, and Y. S. Kwon, Phys. Rev. B **87**, 125121 (2013).

[18] J. N. Kim, C. Lee, and J.-H. Shim, New J. Phys. **15**, 123018 (2013).

[19] H. Lei, K. Wang, and C. Petrovic, J. Phys.: Condens. Matter **29**, 075602 (2017).

[20] A. V. Morozkin and Y. D. Seropegin, J. Alloys Compd. **365**, 168 (2004).

[21] G. Kresse and J. Furthmüller, Phys. Rev. B **54**, 11169 (1996).

[22] G. Kresse and D. Joubert, Phys. Rev. B **59**, 1758 (1999).

[23] P. E. Blochl, Phys. Rev. B **50**, 17953 (1994).

[24] J. P. Perdew, K. Burke, and M. Ernzerhof, Phys. Rev. Lett. **77**, 3865 (1996).

[25] See Supplemental Material at http://link.aps.org/supplemental/10.1103/PhysRevB.101.155140 for (1) the first-principles calculations, (2) calculated electronic band structures and density of states, and (3) spin density distribution and spin configuration of orthorhombic $Sm_2Ru_3Ge_5$. Also see Refs. [26–29].

[26] A. I. Liechtenstein, V. I. Anisimov, and J. Zaanen, Phys. Rev. B **52**, R5467 (1995).

[27] V. I. Anisimov, F. Aryasetiawan, and A. I. Lichtenstein, J. Phys.: Condens. Matter **9**, 767 (1997).

[28] S. L. Dudarev, G. A. Botton, S. Y. Savrasov, C. J. Humphreys, and A. P. Sutton, Phys. Rev. B **57**, 1505 (1998).

[29] W. Tang, E. Sanville, and G. Henkelman, J. Phys.: Condens. Matter **21**, 084204 (2009).

[30] S. Ramakrishnan, A. Schönleber, T. Rekis, N. van Well, L. Noohinejad, S. van Smaalen, M. Tolkiehn, C. Paulmann, B. Bag, A. Thamizhavel, D. Pal, and S. Ramakrishnan, Phys. Rev. B **101**, 060101(R) (2020).

[31] N. S. Sangeetha, A. Thamizhavel, C. V. Tomy, S. Basu, A. M. Awasthi, S. Ramakrishnan, and D. Pal, Phys. Rev. B **86**, 024524 (2012).

[32] C. S. Lue, Y.-K. Kuo, F. H. Hsu, H. H. Li, H. D. Yang, P. S. Fodor, and L. E. Wenger, Phys. Rev. B **66**, 033101 (2002).

[33] M. Murase, A. Tobo, H. Onodera, Y. Hirano, T. Hosaka, S. Shimomura, and N. Wakabayashi, J. Phys. Soc. Jpn. **73**, 2790 (2004).

[34] N. Yamamoto, R. Kondo, H. Maeda, and Y. Nogami, J. Phys. Soc. Jpn. **82**, 123701 (2013).

[35] K. K. Kolincio, M. Roman, M. J. Winiarski, J. Strychalska-Nowak, and T. Klimczuk, Phys. Rev. B **95**, 235156 (2017).

[36] M. Roman, J. Strychalska-Nowak, T. Klimczuk, and K. K. Kolincio, Phys. Rev. B **97**, 041103(R) (2018).

[37] S. Steiner, H. Michor, O. Sologub, B. Hinterleitner, F. Hofenstock, M. Waas, E. Bauer, B. Stoger, V. Babizhetskyy, V. Levytskyy, and B. Kotur, Phys. Rev. B **97**, 205115 (2018).

[38] C. N. Kuo, D. Shen, B. S. Li, N. N. Quyen, W. Y. Tzeng, C. W. Luo, L. M. Wang, Y. K. Kuo, and C. S. Lue, Phys. Rev. B **99**, 235121 (2019).

[39] K. Zhang, X. Liu, H. Zhang, K. Deng, M. Yan, W. Yao, M. Zheng, E. F. Schwier, K. Shimada, J. D. Denlinger, Y. Wu, W. Duan, and S. Zhou, Phys. Rev. Lett. **121**, 206402 (2018).

[40] C. S. Lue, Y. F. Tao, K. M. Sivakumar, and Y. K. Kuo, J. Phys.: Condens. Matter **19**, 406230 (2007).

[41] E. D. Mun, S. L. Bud'ko, and P. C. Canfield, J. Phys.: Condens. Matter **23**, 476001 (2011).

[42] C. S. Lue, S. H. Yang, A. C. Abhyankar, Y. D. Hsu, H. T. Hong, and Y. K. Kuo, Phys. Rev. B **82**, 045111 (2010).

[43] R. T. Littleton IV, T. M. Tritt, J. W. Kolis, D. R. Ketchum, N. D. Lowhorn, and M. B. Korzenski, Phys. Rev. B **64**, 121104(R) (2001).

[44] C. N. Kuo, H. F. Liu, C. S. Lue, L. M. Wang, C. C. Chen, and Y. K. Kuo, Phys. Rev. B **89**, 094520 (2014).

[45] R. Gumeniuk, K. O. Kvashnina, W. Schnelle, A. Leithe-Jasper, and Y. Grin, Phys. Rev. B **91**, 094110 (2015).

[46] C. N. Kuo, C. W. Tseng, C. M. Wang, C. Y. Wang, Y. R. Chen, L. M. Wang, C. F. Lin, K. K. Wu, Y. K. Kuo, and C. S. Lue, Phys. Rev. B **91**, 165141 (2015).

[47] Y. Liu, H. Lei, K. Wang, M. Abeykoon, J. B. Warren, E. Bozin, and C. Petrovic, Phys. Rev. B **98**, 094519 (2018).

[48] Y.-K. Kuo, C. S. Lue, F. H. Hsu, H. H. Li, and H. D. Yang, Phys. Rev. B **64**, 125124 (2001).

[49] Y.-K. Kuo, F. H. Hsu, H. H. Li, H. L. Huang, C.W. Huang, C. S. Lue, and H. D. Yang, Phys. Rev. B **67**, 195101 (2003).

[50] R. F. Luccas, A. Fente, J. Hanko, A. Correa-Orellana, E. Herrera, E. Climent-Pascual, J. Azpeitia, T. Perez-Castaneda, M. R. Osorio, E. Salas-Colera, N. M. Nemes, F. J. Mompean,

M. Garcia-Hernandez, J. G. Rodrigo, M. A. Ramos, I. Guillamon, S. Vieira, and H. Suderow, Phys. Rev. B **92**, 235153 (2015).

[51] A. V. Tsvyashchenko, D. A. Salamatin, V. A. Sidorov, A. E. Petrova, L. N. Fomicheva, S. E. Kichanov, A. V. Salamatin, A. Velichkov, D. R. Kozlenko, A. V. Nikolaev, G. K. Ryasny, O. L. Makarova, D. Menzel, and M. Budzynski, Phys. Rev. B **92**, 104426 (2015).

[52] F. Galli, S. Ramakrishnan, T. Taniguchi, G. J. Nieuwenhuys, J. A. Mydosh, S. Geupel, J. Ludecke, and S. van Smaalen, Phys. Rev. Lett. **85**, 158 (2000).

[53] F. Galli, R. Feyerherm, R. W. A. Hendrikx, S. Ramakrishnan, G. J. Nieuwenhuys, and J. A. Mydosh, Phys. Rev. B **62**, 13840 (2000).

[54] M. H. Lee, C. H. Chen, C. M. Tseng, C. S. Lue, Y. K. Kuo, H. D. Yang, and M.-W. Chu, Phys. Rev. B **89**, 195142 (2014).